Supporting Information for

Two-Dimensional Solid-Phase Crystallization toward Centimeter-Scale Monocrystalline Layered $MoTe_2$ via Two-Step Annealing

Chih-Pin Lin, [a] *Hao-Hua Hsu,* [a] *Jyun-Hong Huang,* [a] *Yu-Wei Kang,* [a] *Chien-Ting Wu,* [b]
Yao-Jen Lee, [b] *Chun-Cheng Cheng,* [c] *Yann-Wen Lan,* [d] *Wen-Hao Chang,* [e]
Lain-Jong Li, [f] *and Tuo-Hung Hou* *[a]

[a]Department of Electronics Engineering and Institute of Electronics, National Yang Ming Chiao Tung University, Hsinchu 300, Taiwan

[b]Taiwan Semiconductor Research Institute, Hsinchu 300, Taiwan

[c]Advanced Technology Research Center, AU Optronics Corporation, Hsinchu 300, Taiwan

[d]Department of Physics, National Taiwan Normal University, Taipei 116, Taiwan

[e]Department of Electrophysics, National Yang Ming Chiao Tung University, Hsinchu 300, Taiwan

[f]Department of Mechanical Engineering, The University of Hong Kong, Pokfulam, Hong Kong SAR, China

*Electronic mail: thhou@mail.nctu.edu.tw

S1. 2H-$MoTe_2$ formation by Using Different Sputtering Time of $MoTe_2$

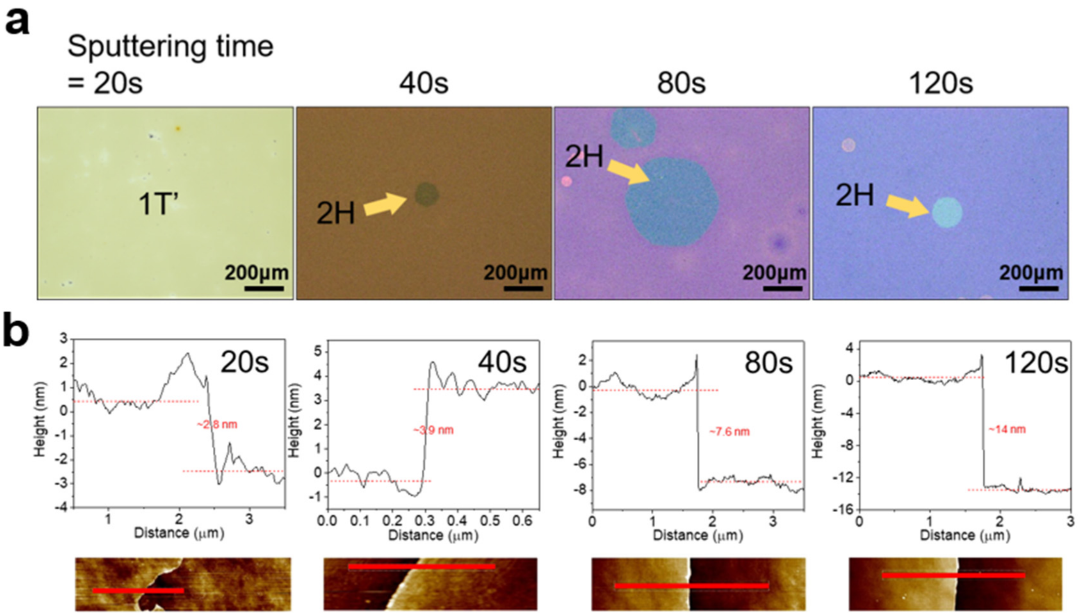

Fig. S1 Optical image of $MoTe_2$ with various sputtering time at T_a = 700 ℃ for 5 min in RTA. The thickness of $MoTe_2$ film is easily controlled by tuning the sputtering time,[1,2] which can be seen also from (a) the apparent color contrast in the optical images and (b) AFM results of as-sputtered $MoTe_2$. The sputtering time of 40s is selected in our study to obtain a thinner thickness.

S2. Temperature-Dependent 2H-$MoTe_2$ Nucleation in RTA

Table S2 Phase of $MoTe_2$ as a function of T_a in RTA with t_a= 1 min.

Temperature (°C)	500	650	700	750	800	850	900
Phase	α	1T'	1T'/2H	1T'/2H	1T'/2H	1T'/2H	1T'

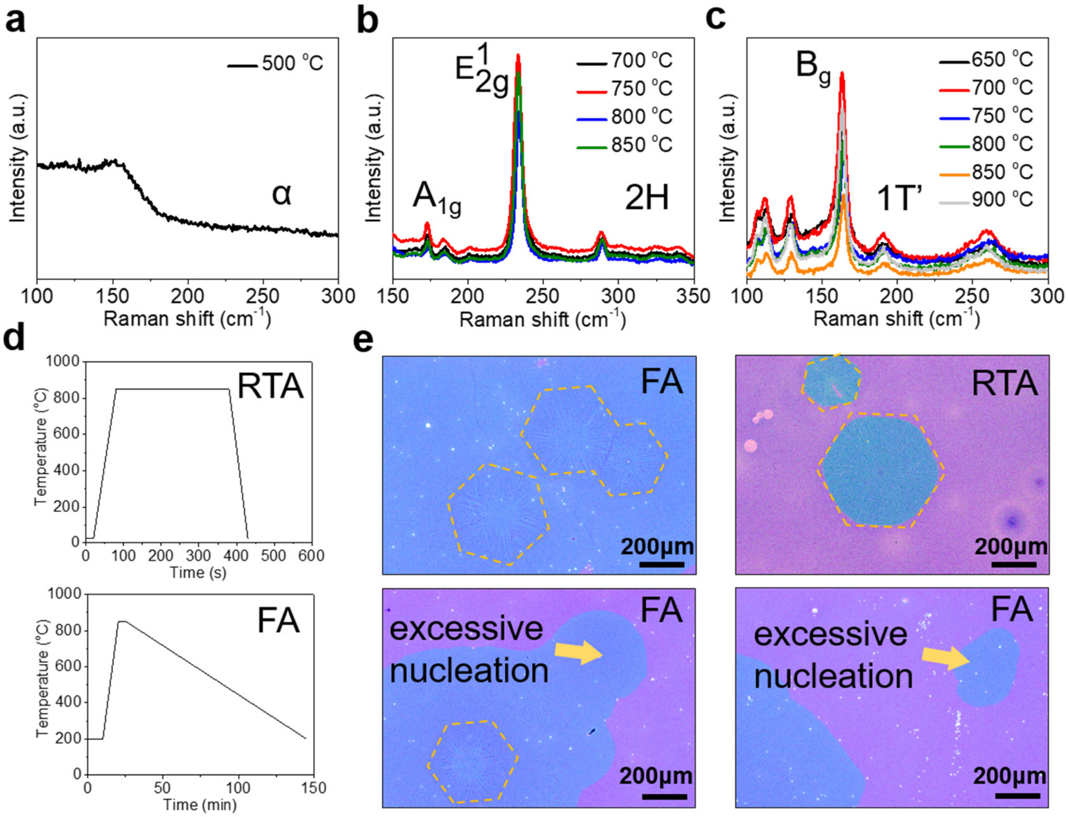

Fig. S2 (a-c) Raman spectra of α-, 2H- and 1T'-phase at various T_a in RTA. (d) Annealing temperature profiles of RTA and FA. The r_{ramp} and t_{cool} of RTA (FA) are 55 °C/s (~1 °C/s) and 20s (~2 hr), respectively. Both t_a and T_a are 5 min and 850 °C. (e) Optical image of hexagonal 2H $MoTe_2$ annealed at 850 °C for 5 min in FA and RTA. Excessive nucleation could be observed in FA-annealed samples due to the slow heating and cooling processes.

S3. Effect of r_{ramp} and t_{cool} on the Synthesis of 2H-MoTe$_2$ in RTA

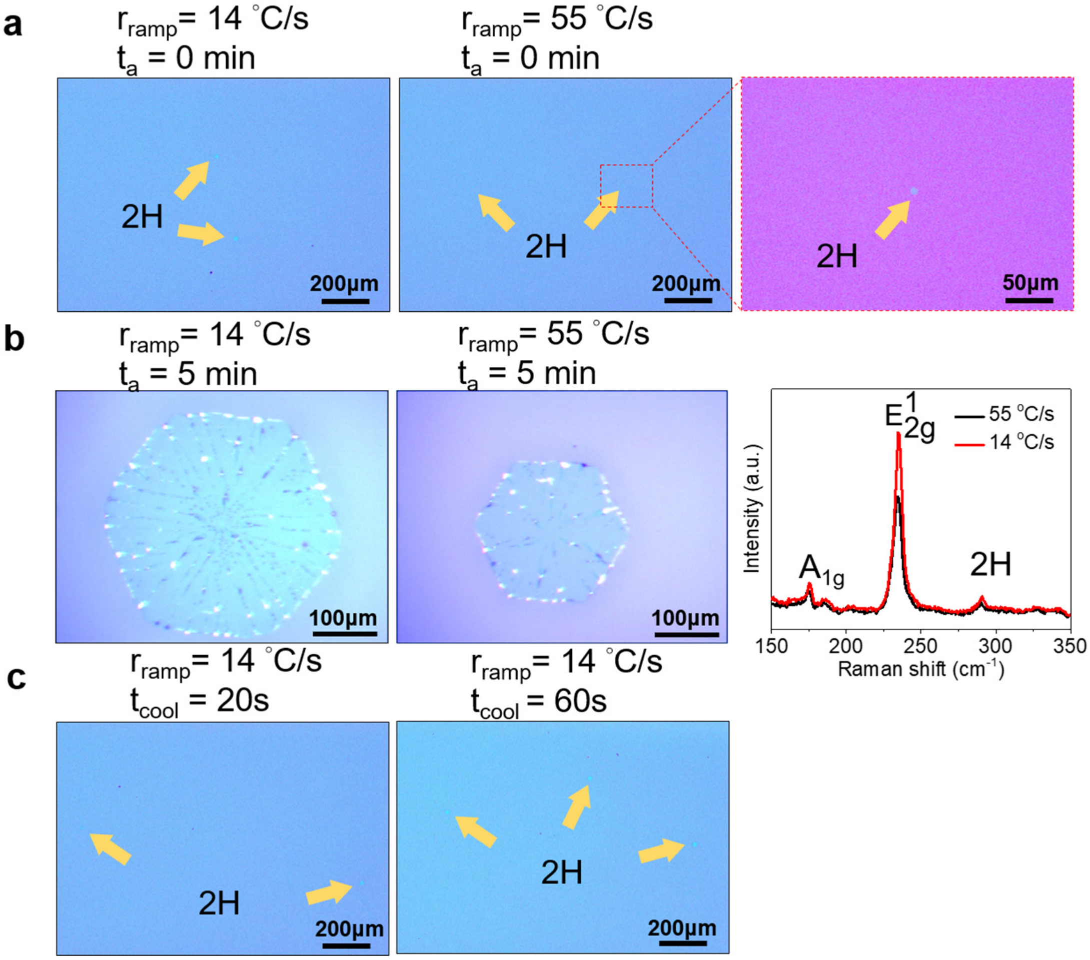

Fig. S3 Effect of r_{ramp} on (a) 2H-phase nucleation and (b) domain morphology. (c) Effect of t_{cool} on 2H-phase nucleation. In the range we chose, both parameters in RTA show insignificant effects.

S4. Effect of t_a on the Domain Morphology

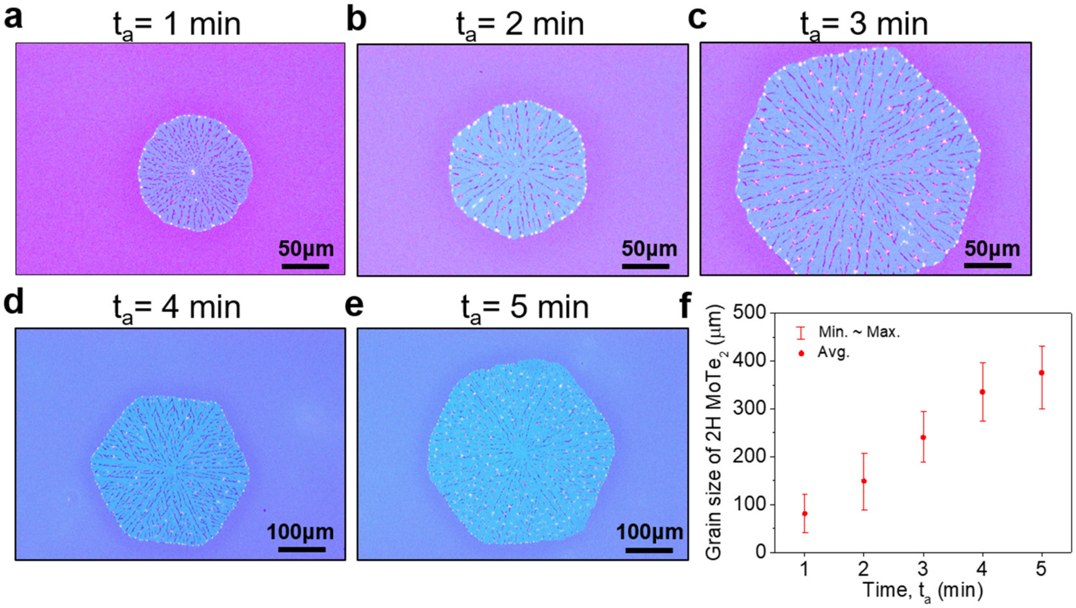

Fig. S4 Time evolution (t_a= 1 to 5 min) of domain (a-e) morphology and (f) size of 2H-MoTe$_2$. The 2H-MoTe$_2$ domain shows a shape transition from round to hexagonal as t_a increases, and the grain size monotonously increases over time.

S5. Crystallographic Orientation of Hexagonal 2H-MoTe$_2$ Domain

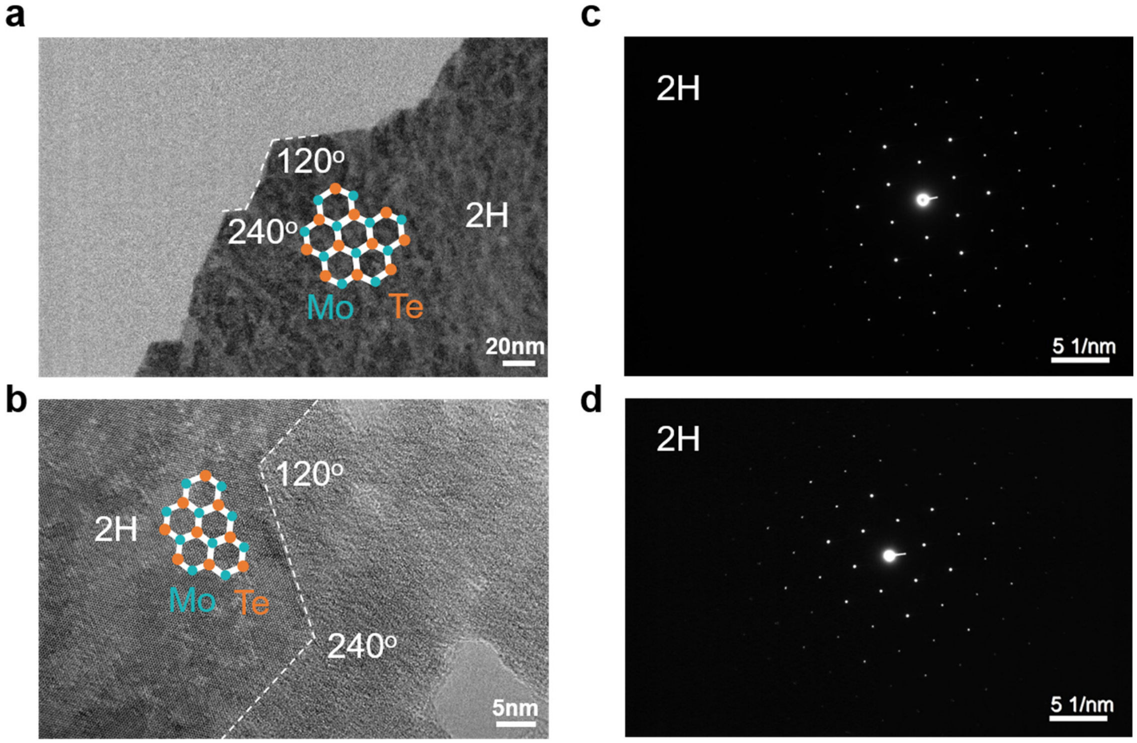

Fig. S5 (a-b) HRTEM image at the boundary of hexagonal 2H-MoTe$_2$ domain and (c-d) its corresponding SAED patterns. Most edge regions show an angle of 120° or 240°, an integer multiple of the angle difference between two adjacent ZZ planes.[3,4] Therefore, we conclude that the hexagonal 2H domain is dominated by the ZZ edges.

S6. Crystallographic Orientation Measured by EBSD

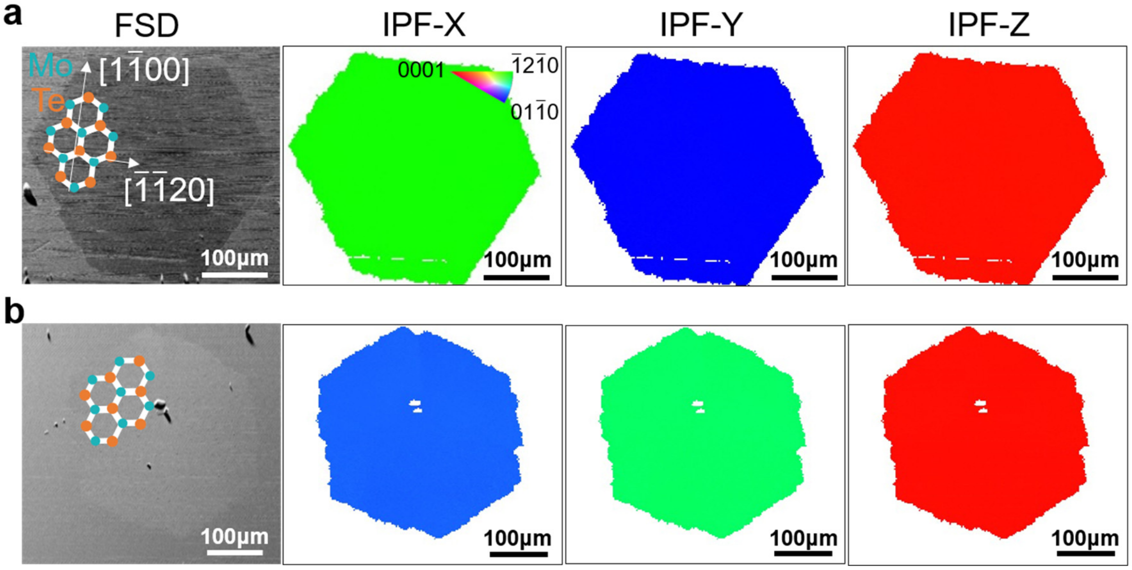

Fig. S6 EBSD mapping of two hexagonal 2H-$MoTe_2$, confirming the crystallographic orientation and monocrystallinity of 2H-$MoTe_2$ domains. All three IPF maps show uniform color distributions, indicating the monocrystalline nature. The color maps of IPF-X and IPF-Y reveal that the crystallographic orientations of hexagonal 2H-$MoTe_2$ are roughly aligned along with the $<\bar{1}2\bar{1}0>$- and $<01\bar{1}0>$-direction corresponding to the x- and y-axis, respectively. The edge is dominated by the ZZ orientation. The IPF-Z also confirmed that the out-of-plane orientation of 2H-$MoTe_2$ is parallel to the substrate in a 2D layered structure.

S7. 2H-MoTe$_2$ Nucleation Sites after RTA treatment

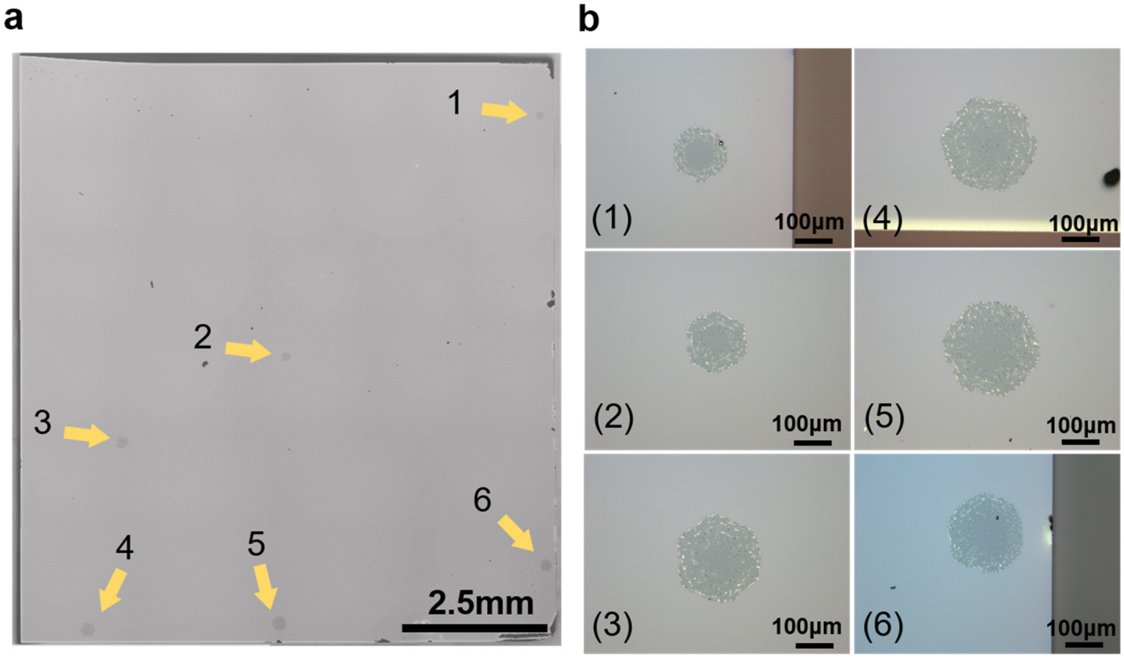

Fig. S7 Optical image showing the distribution of 2H-MoTe$_2$ nucleation sites in α-MoTe$_2$ on a SiO$_2$ substrate (~1 cm^2). The RTA condition was 850 °C for 5 min. r_n is estimated to be 1.2 min^{-1}cm^{-2}.

S8. Estimation of Final Grain Size by JMAK Equation

According to ref. 5, the crystalline fraction (f) of 2D material as a function of time and temperature could be estimated using the Johnson-Mehl-Avrami-Kolmogorov equation:

$$f=1-exp[-Kt^n],$$

where $K=\frac{\pi}{3}r_n v_g^2$, n= 3 in the 2D case. The crystallization time τ is defined by $K\tau{\sim}1$, i.e. $\tau{\sim}\frac{1}{(r_n v_g^2)^{1/3}}$, when the fracture f reaches unity for a completely crystallized film. Therefore, the final grain size could be estimated as $v_g\tau{\sim}\ (v_g/r_n)^{1/3}$. From our experimental results, the mean r_n and v_g of 2H-MoTe$_2$ annealed by RTA are 1.2 min^{-1}cm^{-2} and 0.4 μm/s at 850 °C, respectively. Thus, the final grain size under prolonged RTA treatment is approximately 2.5 mm.

S9. Shape Evolution Using Two Subsequent RTA Treatments

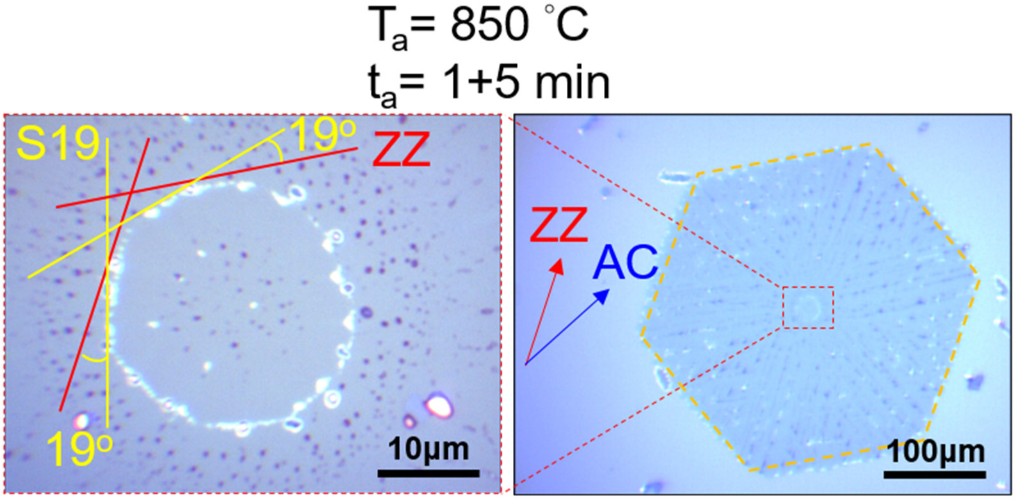

Fig.S8 Shape evolution characterized using two subsequent RTA annealing with t_a= 1 min and 5 min each. The first short-duration RTA produced circular 2H-$MoTe_2$ domains where the edge structure was dominated by S19 (slanted edges with an ~19° angle from the ZZ edge).[6] Such edges were replaced by the ZZ edges after the long-duration RTA for 5 min, and the domain shape was transformed from circular to hexagonal.

S10. Nano-crack Formation in 2H-MoTe$_2$ under High-Temperature SPC

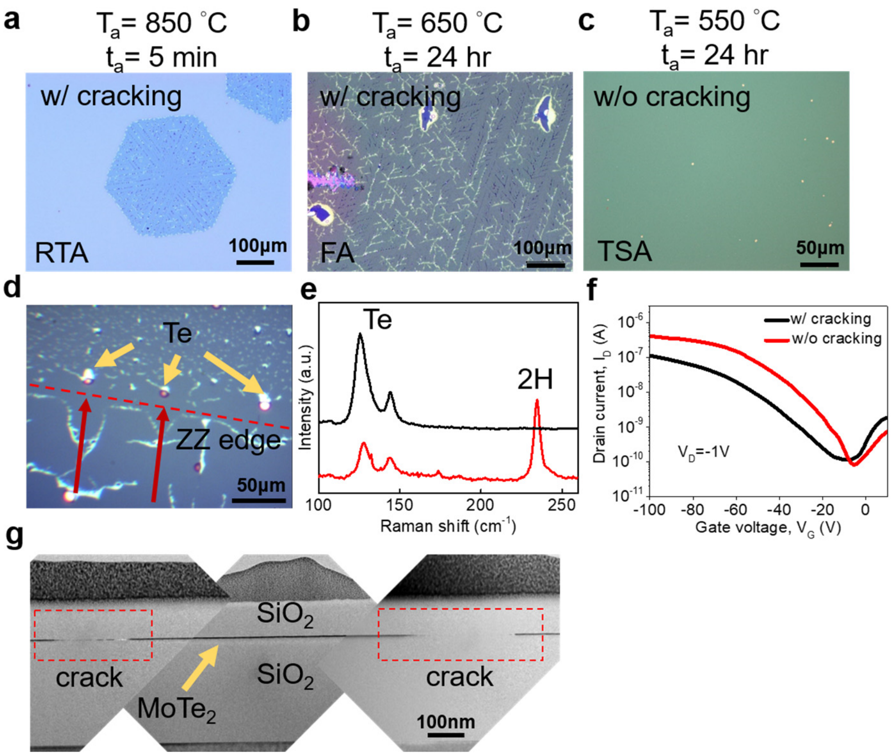

Fig. S9 (a-c) Optical image showing the surface morphology of 2H-MoTe$_2$ annealed by RTA, FA, and TSA. The dendrite-like nano-cracks with a radical pattern were found in 2H-MoTe$_2$ at high T_a regardless of the heating instrument (RTA or FA). (d) Te segregation at the boundary of 2H and 1T' phases. (e) Raman spectroscopy of vibrational modes at ~128 and 145 cm^{-1} confirms the Te segregation.[7] (f) Transfer characteristics (I_D-V_G) of MoTe$_2$ back-gated transistor with and without cracking. The device channel length/width (L/W) is 10μm/24μm. (g) Cross-sectional HRTEM image showing that the nano-crack is due to the local discontinuity of 2H-MoTe$_2$ (the red-dash frame region). The formation of nano-cracks could be suppressed at lower T_a. One plausible explanation of forming nano-cracks is the significant stress induced by the migration of Te clusters at high temperatures during 2H-MoTe$_2$ growth, which might be large enough to rupture the film. In MoS$_2$, a similar stress-induced nano-scratch was observed by applying force using the tip in the atomic force microscope (AFM).[8] The nano-scratchs showed preferable breaking along the ZZ direction since the fracture strength of MoS$_2$ along ZZ is lower than AC. Similarly, the rupture of MoTe$_2$ tends to extend outward along the ZZ direction.

S11. Variation of r_n at Low T_a

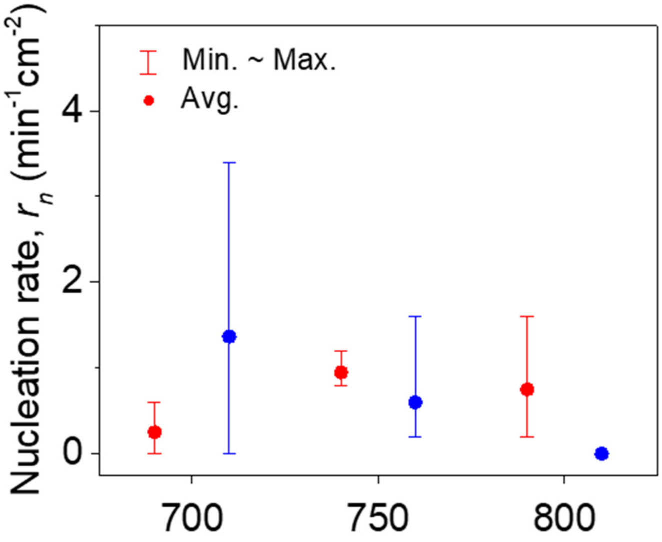

Fig. S10 r_n as a function of T_a in RTA. The statistics of red and blue data are from two different experiments with the same condition. Both experiments show the trend of reduced r_n at higher T_a. By contrast, r_n at low T_a shows large discrepancies between these two experiments. The exact reason is still under investigation.

S12. Monocrystalline 2H-MoTe$_2$ with Different Domain Morphologies

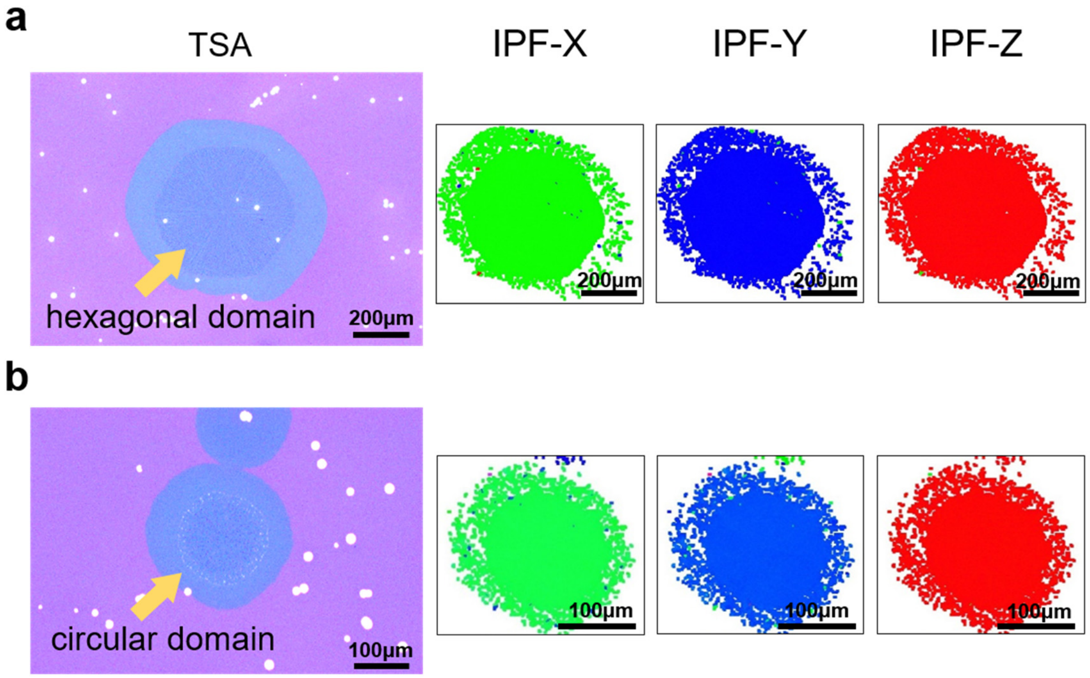

Fig. S11 Optical image and EBSD mapping of 2H-MoTe$_2$ after TSA by using (a) hexagonal and (b) circular domains as seeds. The second-step FA continued enlarging monocrystalline grains outward from the seed regions.

S13. 2H-MoTe$_2$ Transistors with ZZ- or AC Channel Orientation

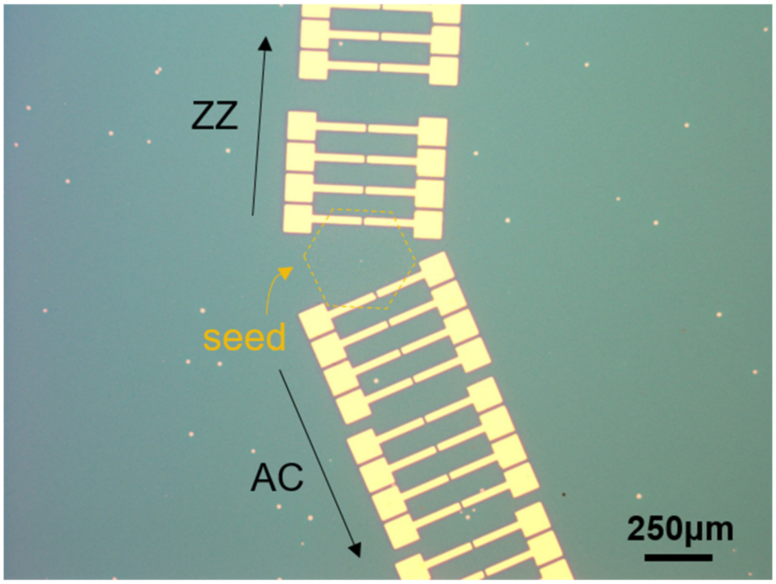

Fig. S12 Optical image of 2H-MoTe$_2$ transistors with ZZ and AC channel orientation in a large area.

References

1. J. –H. Huang, K. –Y. Deng, P. –S. Liu, C. –T. Wu, C. –T. Chou, W. –H. Chang, Y. –J. Lee and T. –H. Hou, *Adv. Mater. Interfaces* 2017, **4**, 1700157.
2. J. –H. Huang, H. –H. Hsu, D. Wang, W. –T. Lin, C. –C. Cheng, Y. –J. Lee and T. –H. Hou, *Sci. Rep.* 2019, **9**, 8810.
3. Q. Yu, L. A. Jauregui, W. Wu, R. Colby, J. Tian, Z. Su, H. Cao, Z. Liu, D. Pandey, D. Wei, T. F. Chung, P. Peng, N. P. Guisinger, E. A. Stach, J. Bao, S. –S. Pei and Y. P. Chen, *Nat. Mater.* 2011, **10**, 443-449.
4. J. H. Sung, H. Heo, S. Si, Y. H. Kim, H. R. Noh, K. Song, J. Kim, C. –S. Lee, S. –Y. Seo, D. –H. Kim, H. K. Kim, H. W. Yeom, T. –H. Kim, S. –Y. Choi, J. S. Kim and M. –H. Jo, *Nat. Nanotechnol.* 2017, **12**, 1064-1070.
5. X. Xu, S. Chen, S. Liu, X. Cheng, W. Xu, P. Li, Y. Wan, S. Yang, W. Gong, K. Yuan, P. Gao, Y. Ye and L. *J.* Dai, *Am. Chem. Soc.* 2019, **141**, 2128-2134.
6. T. Ma, W. Ren, X. Zhang, Z. Liu, Y. Gao, L. –C. Yin, X. –L. Ma, F. Ding and H. –M Cheng, *PNAS* 2013, **110**, 20386-20391.
7. S. Khatun, A. Banerjee and A. J. Pal, *Nanoscale* 2019, **11**, 3591-3598.
8. S. Ye, K. Xu, L. Lei, S. Hussain, F. Pang, X. Liu, Z. Zheng, W. Ji, X. Shi and R. Xu, *Mater. Res. Express.* 2019, **6**, 025048.